High resolution imaging of GaAs nanowires

Bachelor Thesis

Andreas Johansson

Division of Synchrotron Radiation Research
Department of Physics
Lund University

High resolution imaging of GaAs nanowires

Division of Synchrotron Radiation Research
DEPARTMENT OF PHYSICS

Bachelor Thesis

LUND UNIVERSITY

Author: Andreas Johansson
Supervisor: Dr. Anders Mikkelsen
Date: June 21, 2012

Abstract

Semiconductor nanowires (NWs) are expected to be the new building blocks in electronics and photonics, but improved understanding of the nanowire surfaces and electronic properties are required to realize it.

In this bachelor thesis, wurtzite (Wz)-zincblende (Zb) axial heterostructure GaAs nanowires are studied using scanning tunneling microscopy and spectroscopy. The hexagonal cross section nanowires have {110}- type side facets for the Zb top part and {10-10}- type side facets for the Wz bottom part . Additionally {11-20}-type facets and {111}B- type facets are present at the transition between the two crystal structures. The surfaces of these facets are investigated to characterize their morphology and defects.

The {110}-type zincblende facets are characterized by 60-80 nm wide terraces with wavy edges. At least one type of point defects is observed on the surface, which is thought to be Arsenic mono-vacancies with a density of the order 10^{12}-$10^{13}\mathrm{cm}^{-2}$. No stacking faults or twin-planes are observed in the zincblende crystal structure, but are seen in the crystal transition region between the two crystal structures. A downward directed, 5-15 nm wide stripe-like overgrowth structure is seen on the {11-20}-type wurtzite facets. Furthermore, 50-70 nm wide {10-10}-type facets show a morphology of atomic steps occurring perpendicular to the nanowire growth direction. A 5-15 nm wide structure, parallel the nanowires are observed to emanate from these atomic steps. The surfaces of the wurtzite part of the nanowires have almost no point defects, but show a low density of stacking fault.

Contents

1 Introduction

Nanoscience is an active area of research. It deals with materials and their properties at the nanometer ($10^{-9}m$) scale. One particular class of nanometer sized structures studied is III-V semiconductor nanowires. These are thin rod shaped crystals made out of atoms from group III and V in the periodic table. A good degree of control has been gained in semiconductor nanowires synthesis, which has enabled tuning of their electronic properties. [30, 31] It is now possible to obtain nanowires which have different crystal structure in different parts of the nanowire. [5] These nanowire heterostructures have properties which makes them of interest for nanometer scale device applications. [31]

The structure of nanowires makes it possible to integrate them with standard Si technology used in integrated circuits, which provides a great advantage over other nanostructures. [25] Semiconductor nanowires have potential to be used in devices such as nanowire lasers, single electron memories, light emitting diodes (LEDs) and high efficiency solar cells to name a few. [5, 23, 25] GaAs is a semiconductor material which has several advantageous properties, such as high electron and hole mobilities, as well as direct band gaps. These properties make them an interesting nanowire material.

Nanowires are the impressive result of continued miniaturization, but with decreasing dimensions, the surface to bulk ratio increases. The nanowire surface and the morphology of the nanowire therefore become increasingly important for the electronic properties of the structure. Furthermore, surfaces are the place where chemical reactions happen. It is therefore of great importance to improve the understanding of nanowire surfaces by characterizing them, so that engineered devices can be optimized. Careful control of the structure of the nanowires essential to avoid stacking faults and twin planes and other undesired crystal defects which compromise the crystal perfection, upon which the success of further devices depend. [23, 31]

Scanning tunneling microscopy (STM) and spectroscopy (STS) are two surface sensitive techniques used in this experimental bachelor thesis to study the surface of axial heterostructure GaAs nanowires with zincblende and a wurtzite crystal structure in the bottom. The surface of these nanowire facets are investigated with respect to surface morphology, surface defects and crystal defects.

2 Theoretical background

2.1 Scanning Tunneling Microscopy (STM)

The STM was invented in 1982 by Gerd Binning and Heinrich Röhrer (at IBM, Zürich, Switzerland) which earned them the Nobel Prize in Physics in 1986. [1] It is a scanning probe technique based on tunneling of electrons between a sample and a sharp metal tip. It can provide high resolution atomic-scale images of metal and semiconductor surfaces in real space. The up to atomic spatial resolution allows individual atomic bonds within conducting materials to be imaged. [26] This gives valuable information about the local topographic and electronic properties of the scanned surfaces. Amongst other things, the scanning tunneling microscope can be used to determine atomic surface structure and to characterize surfaces by observing defects and reconstructions. [2]

2.1.1 Theory of Operation

The basic elements of the scanning tunneling microscope are an atomically sharp tip, a piezoelectric tube, a current amplifier, a unit for data processing and display, and one for tip-sample distance control.

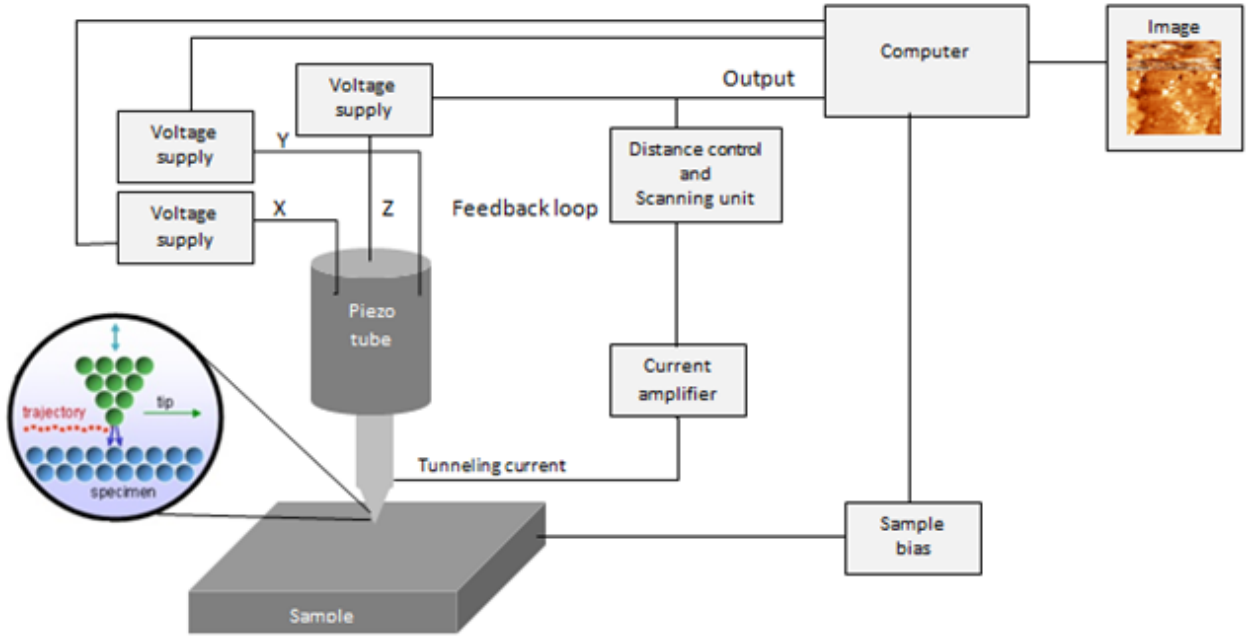

Figure 2.1: Schematic illustration of the principle of operation for an STM setup. A piezo tube controls the motion of the tip over the sample surface. In constant current mode, a feedback circuit compares the measured tunneling current to a pre-set value and adjusts the tip accordingly. The blow-up image shows the trajectory of the tip as it is scanned above the surface. [20] The tip movement can be converted into an image of the surface, displayed by the computer.

The operation of the microscope relies on the tunneling effect, a quantum mechanical phenomenon where electrons in this case, can tunnel through a classically forbidden potential gap.

The idea behind the STM operation is to approach the surface of a sample with a sharp metal tip without crashing into it, until it is within a nanometer of surface. At this distance the electronic wave functions of the tip and the sample surface will begin to overlap so that it becomes probable for electrons to tunnel across the vacuum barrier separating the two. [18] A measurable net current is produced by applying a small tip-sample bias, set by the STM operator, typically in the order of a few volts for semiconductors. Electrons will either flow into the sample or the tip, depending on the sign of the bias applied.

The tip is moved over the surface in a precise manner by a scanner containing piezoelectric elements. [18] Piezoelectric elements change size ($\sim 1\text{Å}/\text{mV}$) when applying a voltage across them. This constitutes the base for the high precision tip placement needed when scanning using STM. [10] The data recording can proceed by two different modes, either by holding the *z*-position of the tip fixed or by holding the tunneling current constant using a feedback loop. The latter is preferred in cases where the surface are not perfectly flat, since it can better avoid crashes into the sample resulting in a blunt tip, incapable of atomic scale imaging. In this mode of operation the tip is scanned over an area of interest while holding the current constant, at value chosen by the operator. In order to keep the current at a constant pre-set value, a feedback loop is used to move the tip up or down relative to the surface by applying a voltage to the *z*- piezo element. [9] The *z*- piezo electric voltage applied is recorded as a function of *x*-*y* position as the tip scans the surface, which can then be translated into a STM image with a color scale representing the height variations. [10]

2.1.2 The tunneling current

The most important quantity of the STM technique is without a doubt the tunneling current I_T. It is the measured quantity, from which the obtained images are constructed. An accurate description of it is therefore necessary to understand what the images represent.

Tersoff and Hamann formulated a model of the tunneling current based on a perturbation treatment of the tunneling current. [28] The model assumes a perfect tip consisting of a spherical apex with s-like wave functions dominating the tunneling current. [29] In their model it is shown that the tunneling current is proportional to the integrated local density of states (LDOS) at the Fermi energy E_F up to $E_F + eV_T$ according to:

$$I_T = \rho_{tip} \int_0^{eV_T} \rho_{sample}(\mathbf{r}, E_F + \varepsilon)\, d\varepsilon$$

Where **r** is the position of the tip and $\rho_{sample}(\mathbf{r}, E_F + \varepsilon)$ is the LDOS at an energy $E_F + \varepsilon$ and position **r**. ρ_{tip} is the LDOS for the tip, approximated as a constant.

The local density of states in the sample gradually drops off to zero outside the sample. To a simple approximation the magnitude of the tunneling current depends exponentially on the tip-surface separation *s* through an exponential decay of the LDOS into the vacuum.

The exponential dependence on the tip-sample separation results in a very high (typically <0.1Å) resolution perpendicular to the surface. [10]

The sample bias and tunneling current parameters for the STM is set by the operator, as inputs to the computer. By changing the voltage, the electronic states which can contribute to the tunneling current are determined. The STM images on the atomic scale should thus be seen as a map of the local density of states near the Fermi level, of the sample. [18].

When applying a negative bias to a semiconductor sample, electrons in the conduction band of the material will be inclined to 'jump' to the lower lying unoccupied states of the tip. If a positive sample bias is applied, the transfer of electrons will instead go from states in the tip to unoccupied valence band states of the sample. The sign of the applied bias thus decides if empty or filled states of the sample will be imaged. [26] In III-V semiconductors empty states are thought to be localized at dangling bonds of the group III and the filled states at the group V-atom. [8, 24] The sign of the bias used when imaging therefore decides which sub lattice that is imaged.

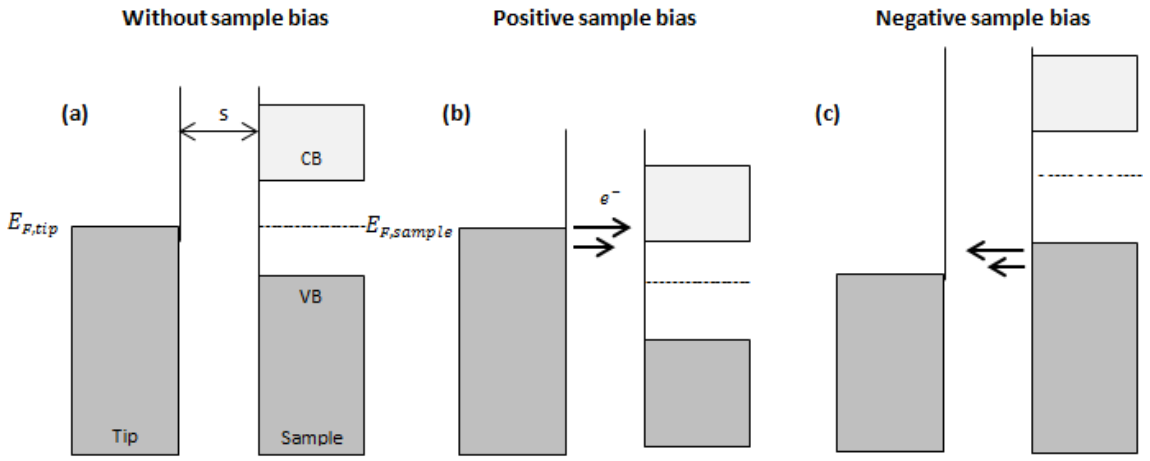

Figure 2.2: Figure showing a simplified view of the tunneling of electrons between a metal tip and a semiconductor surface for zero, positive and negative applied bias respectively. The shaded areas represent the occupied states. The valence band and conduction band of the semiconductor are marked VB and CB respectively. E_F marks the Fermi energy level of the tip and the sample, and *s* is the tip-sample separation.(a) With zero applied bias, the Fermi level of the sample respectively and the tip are aligned resulting in no net current . (b) Under positive sample bias, a flow of electrons will appear from the tip to the conduction band of the sample. (c) Negative sample bias results in tunneling of electrons from filled states in the valence band of the sample into the tip.

2.1.3 Interpretation of images

The interpretation of an STM image is far from trivial. To be able to interpret an image correctly, it is important to understand how it is produced. The image represents variations in *z*-position of the tip as it is scanned over the surface, while obtaining a constant current. As concluded in the previous section, the tunneling current is related to the local density of states in the tip and the sample. This means that the image represents the local electronic properties of both the tip and sample.

However, the shape of the tip as a whole can greatly influence the image, if it is not perfectly sharp and stable. It is therefore of great importance to scan with a sharp, ideally an atomically sharp tip. It is often the case that the tip is not perfect, resulting in images with features related to the tip rather than the sample. Interpretation of an image can be separated into interpretation of larger scale features and atomic scale features.

As long as the image features are in the nanometer range or larger, the images produced can to a good degree be seen as topological representations of the samples morphology. [8] Effects related to the tip shape can however be noticed. One example is that of imaging with a blunt tip. When the tip is large compared to the structure one wants to image, the result is an increased apparent size of the imaged object. Such a tip is unable to resolve smaller topographic changes, which instead may appear as flatter and wider that they are. One such an example is shown below in figure 3.3 (a).

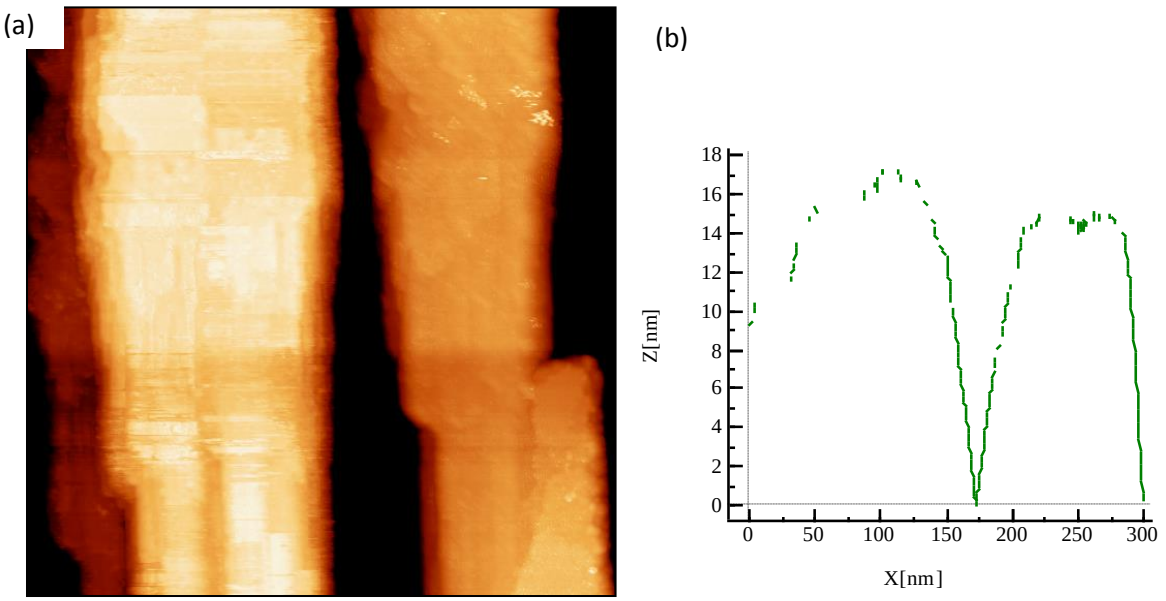

Figure 2.3 (a) 300x300 nm^2 image of a pair of close laying nanowires, imaged with a slightly blunt tip. Due to the shape of the tip, the imaged nanowires are imaged to be wider than they are. It is also possible that the nanowire to the left is imaged with more than one part of the tip, generating reappearing features. (b) 300 nm long line profile perpendicular to the nanowires in a), showing the cross section of the imaged nanowires. Due to the bluntness of the tip, it is unable to reach down and image in between the nanowires, resulting in a decreased cross sectional height of the structures.

When imaging features on the atomic scale, it is no longer possible to interpret the image directly as a topological map of the surface. [10, 30] Electronic properties of the sample as well as the tip must be taken into account. It is therefore the case that the often changing condition of the tip, through changing density of states near the Fermi level of the tip, is reflected in the images.

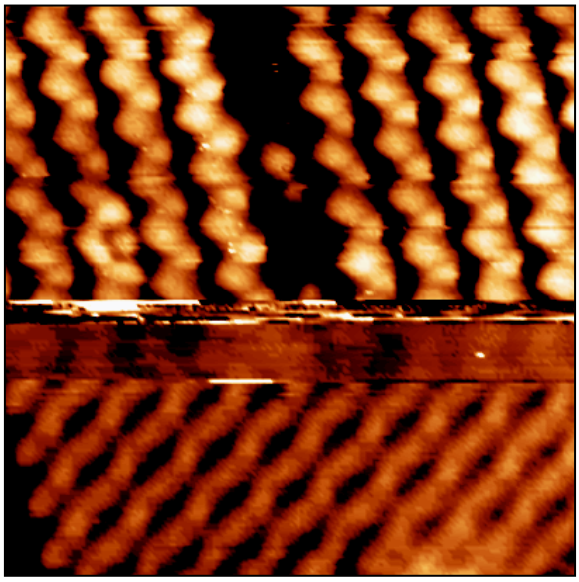

Figure 2.4 7x7 nm^2 atomic scale image showing the effect of a change in the tip while scanning. Through the changed tip state, the expected atomic structure of the upper part of the image is replaced by another pattern, which do not correspond to the atomic structure of the sample at that area. The image was taken with an applied bias of $V_T = -2.5$ V and a tunneling current $I_T = 100$ pA

Another common example of tip induced effects is when tunneling of electrons proceeds to two or more apexes of the tip, instead of one. Features will then appear multiple times in the image, with some separation corresponding to the separation of the multiple tip structure. With such a tip, the sensitivity to variations in height is also partly lost. This effect comes from the fact that the 'demanded' current can come from any of the multiple-tips and may change during the scanning process.

STM images can apart from tip induced features also be plagued by non-linear piezo response. The response of the piezo scanner elements to an applied voltage is not always linear and matching the calibration. Images taken before the piezo-scanner has stabilized after expending/contracting are often seen to be stretched or contracted due to a drift of the scanner.

When imaging semiconductors, variations with the applied voltage can also be seen in the images. This means that the topology is easier deduced by taking images of the same area with different applied voltages. This idea is used in the technique of scanning tunneling spectroscopy.

2.2 Scanning tunneling spectroscopy (STS)

An STM image does not always give the surface structure as concluded in the previous section. The reason is that apart from tip artifacts, the imaged features are voltage-dependent.

STS is a technique used to determine the local electronic properties of a material. [8] Information about the surface can be obtained by probing the electronic properties around the Fermi level. This is done by continuously varying the applied bias of the STM.
In scanning tunneling spectroscopy the feedback loop of the STM is disconnected and the tip is placed in an area of interest, at a fixed tip-sample distance. [11] Then the tunneling current is measured while the voltage is swept through a preset range. The result from such a measurement is a current-voltage curve (*I*-*V*-curve). Only states lying between the Fermi level and $E_F + eV_T$ contribute to the tunneling current as discussed in section 2.1.1.

From the *I*-*V*-curves it is possible to determine the size of the band gap of the investigated semiconductor. The Fermi level, always found at zero applied voltage, will either lie closer or further away from the valence and conduction band offsets depending on the doping. [8] Thus making it possible to deduce information about the doping of the surface.

While *I*-*V* curves give valuable information, it's the differential conductance $\frac{dI}{dV}$ that is directly related to the quantity of interest, the local density of states. [17] Therefore, in addition to the *I*-*V* spectrum one measures the differential signal.

A drawback of the usual type of STS is that, as the voltage is scanned at low voltages, the measured current becomes very small. This leads to reduced accuracy at the band edges and in the band gap where the measured current is close to zero. To overcome this problem Mårtensson and Feenstra presented a technique in 1989, which makes use of a variable tip height. The measurement proceeds in the same manner as the regular STS, but instead of using a fixed z- position of the tip when sweeping the voltage, the tip-sample distance is decreased in a precise manner as the magnitude of the voltage decreases. This approach leads to a larger measured tunneling current and thereby higher accuracy.

By normalizing the differential conductance spectra obtained with variable *z*-mode to the broadened total conductance $\overline{I/V}$, a quantity proportional to the local density of states is formed and at the same time the dependence on the tip-sample separation vanishes. [8]
The result from the treatments mentioned above are a diagram showing $\frac{\frac{dI}{dV}}{\frac{I}{V}}$ against *V*. From these diagrams important features such as band gap edges and surface states can be identified. The spectroscopic information contained in a diagram is provided from a local region 5Å around the point at which the STS was performed. [17] Via the connection to the STM images of the region of the STS spectra, it's possible to identify the influence of defects and adsorbents. [13]

2.3 Nanowires

A nanowire is a nanostructure, typically with a diameter of tens of nanometers. The nanowires are rod shaped with a length to width ratio typically much above 10, which makes them a 1D structure with large surface to bulk ratio. Different types of nanowires exist. They can be free standing or incorporated in a bulk material, consist of a single material, be either axial or radial heterostructures. [4, 5]

As stated previously, the nanowires investigated in this thesis are hexagonal cross section III-V semiconductor GaAs nanowires with a diameter of a few tens of nanometer and with a length in the order of a micrometer. They consist of a two axial crystal structures; zincblende and wurtzite. [7]

2.3.1 Crystal structure

Nanowires grown via an epitaxial technique adopt the crystal structure of the substrate, but by changing growth parameters it's also possible to change from one crystal structure to another during the growth, realizing heterostructures such as the nanowires studied in this thesis.

GaAs along with many other semiconductor materials crystallize naturally with the favored cubic zincblende crystal structure. In the form of nanowires however, crystallization in hexagonal wurtzite crystal structure is also possible. The difference between the two structures is due to differences in the stacking sequences of bilayers.

A bilayer is defined as a double layer of closely packed atoms, which in a III-V material is given by a pair of one group III and one group V atom. The zincblende stacking sequence is ABCABC and ABABAB for wurtzite seen from the growth direction. [23] Here A, B and C denotes three different bilayers or atomic stacking positions. The ABCABC stacking results in a cubic structure whereas ABABAB stacking yields a hexagonal structure.

When the stacking sequence of either the Wz or Zb is interrupted, crystal defects such as stacking faults and twin planes can arise. When a bilayer is misplaced in a wurtzite sequence it gives rise to the following stacking order: AB<u>ABC</u>BCB, which consists of a single segment of zincblende. When a single misplacement happens in the zincblende structure the result is instead a twin plane sequence ABCACBA. A twin plane is defined as two mirror segments rotated with respect to each other. [23] Only when two sequential misplacements of bilayers occur does a wurtzite sequence appear.

The wurtzite crystal structure has a hexagonal crystal unit cell in which the group III and V atoms each form hexagonal close packed (hcp) sub lattices displaced with respect to each other. [14] For the present case these sub lattice consists of a Ga respective As atoms, which are covalently bound to four atoms of the opposite kind. These are coordinated at the edges of a tetrahedron. The hexagonal unit cell is characterized by two lattice parameters; *a* and *c.* The ratio between these parameters are $\frac{c}{a} = \sqrt{8/3} \approx 1.633$ for the wurtzite unit cell. [14]

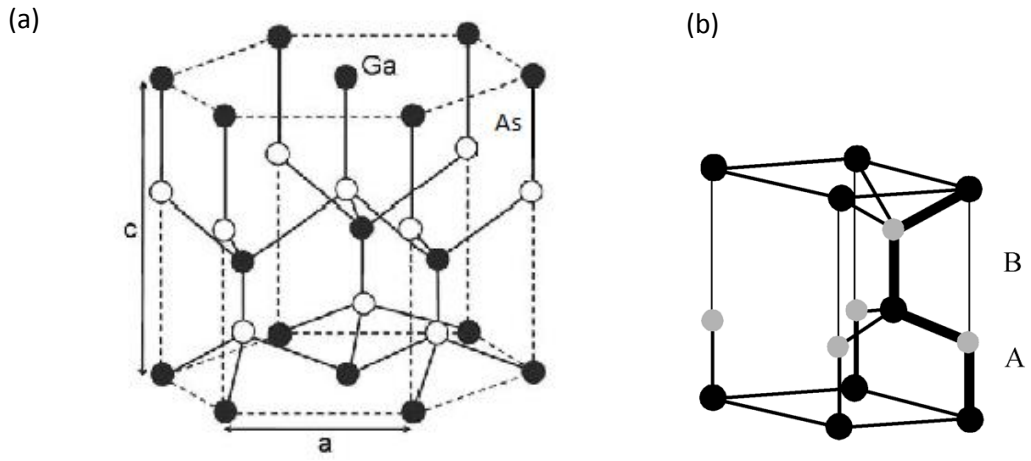

Figure 2.6: (a) Hexagonal wurtzite crystal structure with indicated lattice parameters *c* and *a.* [2] (b) Unit cell for wurtzite showing the stacking sequence viewed normal to the [0001] direction. The bold lines represent bonds lying in the (11-20) plane. [14]

By cleaving the wurtzite crystal in different planes one can obtain crystal planes which appear as facets for the nanowires. One set of such crystal planes are the {10-10}- type which in figure 2.4 (a) can be seen as the set of planes that constitutes the vertical sides of the hexagonal structure. If one rotates the crystal structure and makes a cut, {11-20}- type crystal planes are obtained. Both types mentioned above are seen as nanowire facets for the studied nanowires.

The zincblende crystal structure on the other hand, has a cubic unit cell. It is obtained by stacking two face centered cubic (fcc) lattices into each other, displaced by ¼ of the diagonal distance. [3] The two fcc lattices consist of anions (As) and cations (Ga) respectively. This results in each atom having four atoms of the opposite type as nearest neighbors located on the edges of a regular tetrahedron, just like in the wurtzite crystal structure. The lattice parameter that characterizes the cubic zincblende unit cell is denoted by *a*.

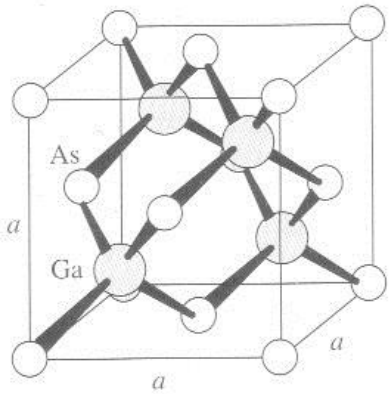

Figure 2.7: Cubic zincblende crystal structure with lattice parameter *a*. [3]

The crystal structure can also be a mixture of zincblende and wurtzite so called polytypic crystal structure, in non-optimized nanowires. Stacking faults are then often connected to alternating segments. [8]

2.3.2 Nanowire facets

Nanowires show facets of different crystal planes. The studied hexagonal cross section NWs have {110} side facets for the zincblende and {10-10} and {11-20} side facets for the wurtzite structure and {110} and {112} facets for the zincblende structures. [15] These facets can all be distinguished using STM because their atomic structure differs.

The {11-20} facets shows zig-zag rows along with the nanowire while the {10-10} facets show rows perpendicular to the nanowire growth direction. The zincblende {110} facet shows rows lying diagonal to the nanowire while the {112}, just like the {10-10} has row perpendicular to the NW. Atomic or near atomic resolution is needed in order to distinguish the different facet types for the wurtzite and zincblende structure.

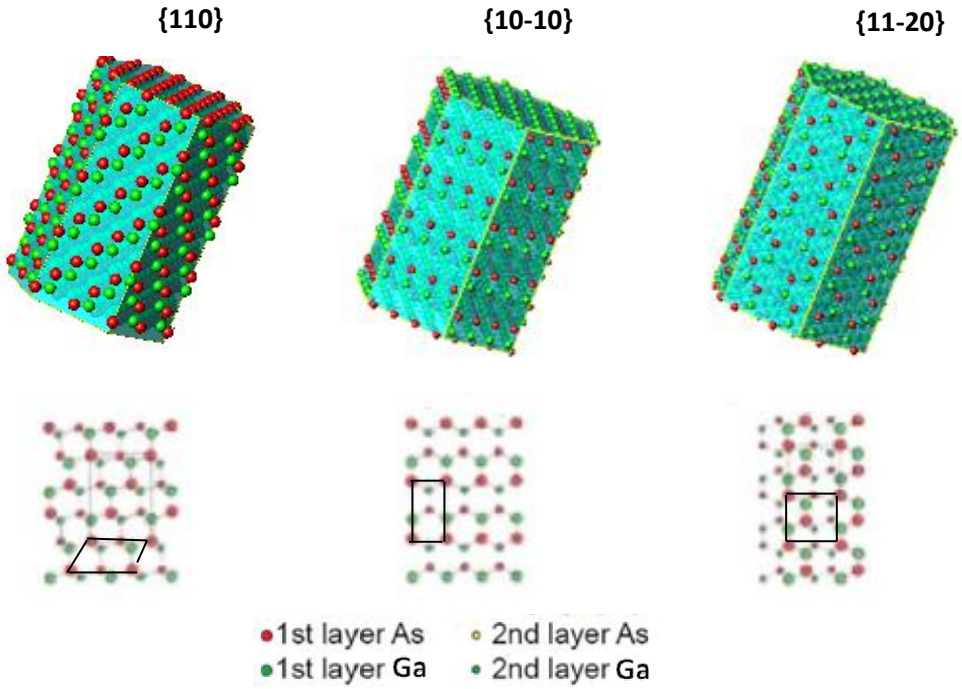

Figure 2.8: Structural 3D model of the three most commonly observed facet types for the studied GaAs nanowires. The {110} zincblende facet is seen to have atomic rows of As and Ga lying on the diagonal, while the {10-10} wurtzite facet shows rows of As respective Ga that lays perpendicular to the nanowire. The {11-20} wurtzite facet has characteristic zig-zag rows along the nanowire direction. The lower images show the atomic structure for the first two atomic layers of the corresponding facet types. [8, 17]

Additionally (111)B type facets for the zincblende type are possible. This cleavage plane (-1-1-1) is group V terminated and by convention called (111)B. [25]

2.3.3 Nanowire growth

Nanowires can be synthesized using a catalyst particle to assist growth on a crystalline substrate (Wagner 1970). Different epitaxial nanowire crystal growth techniques exist; these include chemical beam epitaxy (CBE), metalorganic vapor phase epitaxy (MOVPE) and molecular beam epitaxy (MBE). [4]

One way to synthesize semiconductor nanowires is by depositing gold nanoclusters onto a substrate, which can catalyze a growth via a vapour-liquid-solid process. [5, 33] The substrate commonly used to grow nanowires is the (111)B, because nanowires preferentially grow perpendicular out from such a surface. [4]. The catalysts used to grow the nanowires studied in this thesis, were gold particles with diameters ranging from 20-80 nm which were deposited on a GaAs(111) growth substrate. [7]. The vapour-phase source materials used to grow the nanowires are metal-organic compounds and hybrids in MOVPE, a technique used to grow the nanowires investigated in this thesis. [7]

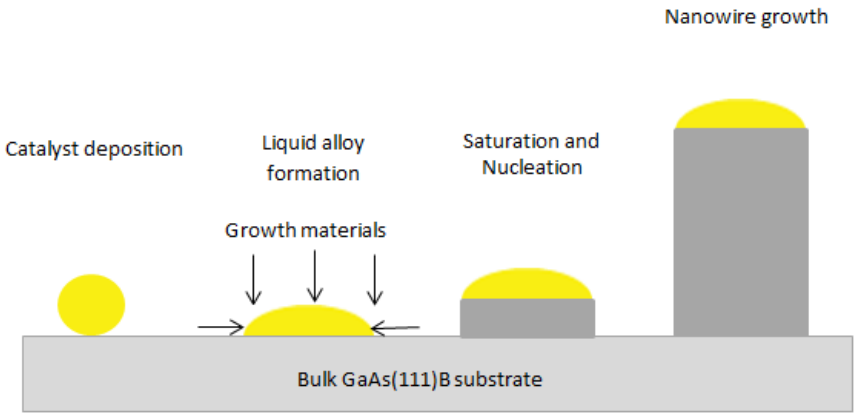

Figure 2.9: The Vapor-Liquid-Solid growth mechanism shown in a few simplified stages. The stages of catalyst deposition, liquid alloy formation, nucleation and axial growth are shown.

After the nanoclusters are supplied to the substrate placed in a growth chamber, it is annealed to remove oxides. The first stage in the growth process is to supply vapour-phase growth materials in the growth chamber. The growth material is adsorbed by the catalyst particles on the substrate at a certain growth temperature. This will lead to a formation of a liquid metal-semiconductor alloy. [5] Continued adsorption of growth materials gives rise to nucleation of solid semiconductor at the liquid/solid interface under the gold particle. The solid semiconductor surface in contact with the liquid metal-semiconductor constitutes the growth interface, and therefore the size of the catalyst particle determines the nanowire diameter. By continuously supplying vapour, a diffusion process will move the semiconductor material from the surface of the liquid gold particle to the growth interface. [5] In the last stage, the axial growth of the nanowires, the vapour will be exposed to both the semiconductor surfaces of the growing nanowire and the metal-semiconductor liquid.

Depending on if the reactant is preferentially incorporated only at the metal-semiconductor liquid or at the solid semiconductor surfaces, growth will happen preferentially in the axial or in the radial direction. The result is crystalline nanowires that will grow up from underneath the liquid gold particles. By changing the different parameters relating to the supplied reactant during the growth process, it's possible to realize axial and radial heterostructures. [8] It should be noted however, that the growth process is not fully understood at present and much remains to be characterized.

3 Experimental methods

3.1 Experimental apparatus

The experiments are performed using an Omicron STM operating at a base pressure $<10^{-10}mbar$ and at room temperature. The system is divided into two main parts, a preparation chamber and an analysis chamber.

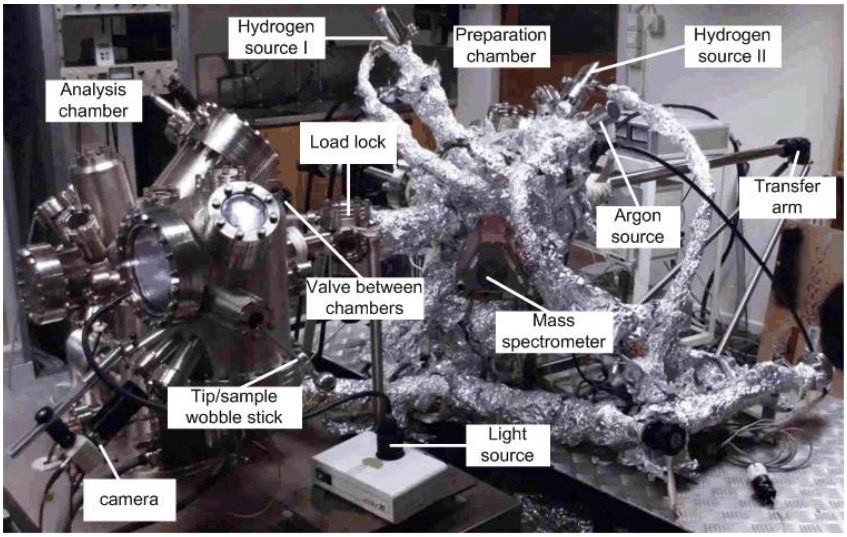

Figure 3.1: The Omicron scanning tunneling microscope used for the experiments. [21]

The preparation chamber and the analysis chamber are separated by a valve sealed tight with copper gaskets, preventing any gas leakage. Both chambers are held at ultra-high vacuum (UHV) pressures by turbo and ion pumps. The valves are sealed tight with copper gaskets, preventing any gas leaking into the chambers. The turbo pump is a mechanical pump with can bring the pressure down to 10^{-8} mbar. From there on, a vibrationless ion pump brings the pressure down two orders of magnitude further. Through the middle of the preparation chamber goes an axis on which a magnetic transfer arm can be used to move things between the chambers.

The preparation chamber is used for sample and tip preparation for later use in the analysis chamber. Connected to the preparation chamber is a hydrogen source used for cleaning the nanowire samples from oxide and an Argon source used for sputtering the STM tip. The setup also includes a mass spectrometer which can be used to determine the composition of gases inside the preparation chamber. To monitor the pressure in the vacuum chambers, two pressure gauges are used. On the central axis between the chambers is a load lock. Through the load lock, samples and tips are inserted into the preparation chamber.

When a sample or tip is ready to be used in an STM measurement, the valve between the chambers is opened for transfer into the analysis chamber where the actual experiment takes place. From the transfer arm, the sample/tip can be placed on holder. Using a wobbler stick, a sample or a tip can be moved from this holder to the final destination on the STM stage which is magnetically damped to reduce transmittance of vibrations. On this stage the tip and the sample are positioned with the help of a camera, a light source and a screen. In the analysis chamber up to 12 different samples/tips can be stored in a ´carousel´ for later use.

An STM image can take anything from under a minute up to an hour to record, and a STM measurement can in total take several days. In order for the nanowire samples to stay free of contaminants during this time period, the STM is operated in an ultra-high vacuum chamber with a base pressure below $10^{-9} - 10^{-10}\mathrm{mbar}$. During the measurements, no vibrations should be transmitted to the tip, because it destroys the resolution of the STM images or result in tip-sample crashes. The system is therefore damped against any vibrations by placing it on a vibrationally damped table and by the use of a magnetic damping system.

3.2 Sample & tip preparation

The as-grown nanowires point perpendicular out from the growth sample and are exposed to air. For these reasons the nanowire surfaces cannot be studied until the nanowires are broken off, placed on another substrate and cleaned from oxide.

The first step in preparing a sample for use in STM is to transfer the nanowires onto another substrate. A GaAs substrate was chosen to avoid contaminating the nanowires with materials other that GaAs which could change the properties of the NW surfaces. The transfer is done by gently placing the growth substrate with nanowires in mechanical contact with the new substrate and after that, a small pressure was applied. The result is a new substrate with a high density of broken-off nanowires deposited in a uniform manner without bundling and with few contaminating fragments. [17] The sample plate is then carefully glued to a sample holder using Indium with low melting point. After this is done, the sample holder with the sample is ready to be inserted into the load lock of the STM.

To image nanowires using an STM, one needs a sharp, high quality tip. Such tips are in this thesis produced via electro-chemical etching from a tungsten wire. The electrochemical etching is done by holding a tungsten wire dipped below the surface of a sodium hydroxide (NaOH) solution while applying a voltage between the wire and a cathode. After 10-20 minutes the lower part of the tip falls off. The remaining part is sharp enough to be used as a STM tip. Before it can be used, it must be cleaned from contaminations from the etching process. This is done by rinsing with isopropanol and distilled water.

To improve the sharpness of the tip further, the tip is placed in the preparation chamber and sputtered with argon ions. The argon is introduced to the preparation chamber by the Argon source at a voltage of 3 kV. The Argon gas is ionized by running a current of 19 mA through a filament. The sputtering process is done at a pressure of $2 \cdot 10^{-6}\mathrm{mbar}$ and it takes about 20 minutes. The sputtering is done twice, one for each side of the tip. This process is also repeated when the quality of the tip is reduced after using the tip for some time.

3.3 Nanowire surface cleaning

In order to study clean nanowires using a scanning tunneling microscope, they first need to be transferred from the growth substrate onto a new substrate. While this could in principle be done in vacuum to prevent any oxidation and contamination of the sample, it would be more complicated and demand some extra effort. Instead one can do the sample preparation in air and then clean the nanowires. This method is used in this thesis.

When brought into air, the nanowires sample oxidizes. The result is a 1-2 nanometer thick layer of native oxide. [8, p. 31] This is a problem, because the STM technique is based on measuring a tunneling current between the sample and the metal tip. Samples with nanowires therefore need to be cleaned from insulating oxides at the surface. The cleaning process must not alter or destroy the surface to be investigated.

The conventional method for cleaning samples is via thermal cleaning. The idea is to heat up the sample in ultra-high vacuum (UHV), at a certain temperature until the oxides desorbs from the surface. Special care must be taken not to exceed the maximum temperature for congruent evaporation, in order to conserve the high crystal quality. If the temperature used for cleaning exceeds this temperature the surface will be destroyed because of preferential evaporation of the group V atoms in the semiconductor material. [4] For GaAs the congruent evaporation temperature is 650°, varying slightly for the different nanowire facets. [4] Above this temperature Ga droplets form, these alter the surfaces chemical composition. The temperature used for cleaning the nanowire samples was therefore chosen to be well below this temperature, yet high enough for oxides to desorb.

In this thesis, a refinement of the standard method is used. The sample is annealed while at the same time exposing it to atomic hydrogen. [16] In this method, hydrogen gas is thermally cracked in a hydrogen source. When the H radials are introduced to the preparation chamber they will react with the oxide on the sample surface and form water and other compounds that desorb at lower temperatures than the congruent evaporation temperature for the nanowire surfaces. [6] Since this method allows for lower cleaning temperatures, it is the method of choice.

The sample is cleaned from native oxides on the nanowire surfaces by annealing with atomic hydrogen at a temperature of around 500°C, a hydrogen pressure of $2 \cdot 10^{-6}$mbar and an annealing time of 20 minutes. When residue oxide and dirt was found on the nanowires, adjustments on the time were done in order to obtain clean nanowires. When a sample is

cleaned it's kept in UHV so that the re-oxidation is slow. At a pressure below $10^{-10}\mathrm{mbar}$ as in the analysis chamber, it takes up to a week before it needs to be cleaned again. During the cleaning process, the molecular hydrogen is introduced by a hydrogen source and is thermally cracked into atomic hydrogen by passing it though a Wolfram filament/tube.

The result of the first cleaning process of the GaAs nanowires on a GaAs(111)B substrate was successful, even though it's known that nanowire surfaces are harder to get clean than other surfaces. Since the substrate and nanowires are made out of the same material in this case, the cleanliness of the substrate serves as a first indication of how successful the cleaning was. The first few images taken after the cleaning were overview images of the substrate. These indicated that the substrate were clean and appeared to have semi-ordered trimers but no droplet formation. This indicated a successful cleaning, which was confirmed when scanning was performed on top of the nanowire surfaces. It was seen that the nanowires were clean for the most part, showing but small traces of residue oxide. Further cleaning processes were performed with the same parameters and yielded similar positive results.

3.4 Imaging of nanowires

Measurements on nanowires are challenging for several reasons. To begin with, a nanowire must be located and identified on the sample surface. This must not take too long a time; else the measurement process will be inefficient and the initially clean sample will become contaminated by adsorbents. The density of nanowires deposited on the sample should therefore be high enough.

Secondly, when doing STM measurements on nanowires, the height difference can be more than 100 nm. The most common way to use STM, is for scanning on very flat surfaces. Height difference of more than a few nanometers can be problematic. Extra measures are therefore needed in order not to crash into the sample when imaging nanowires. A fast STM feedback loop is necessary for the tip to respond quickly to huge height changes. This is ensured by setting the gain parameter of the feedback loop to a high value. The downside of this approach is that the system becomes more sensitive to vibrations, leading to a measurement with more noise. When doing cross sectional imaging of the nanowires, a slow scanning speed must be chosen to lower the risk of crashing into the NWs.

However, imaging of nanowires usually takes place on the top facets of them where they are relatively smooth and suited for scanning. This allows for use of lower values of the gain parameter and faster scanning. Since the pre-set current is closely connected to the tip-sample separation, this parameter can also be adjusted by the operator in accordance with the situation.

Another issue when imaging nanowires is that the nanowires sometimes stick to the tip and are dragged along with it. [9] This is a problem, because it makes it difficult to image on top of the nanowire where one typically wants to image. A voltage pulse of a few volts applied to the tip, can often rid it of nanostructures picked up from the surface.

4 Results and Discussion

As results from the STM measurements, images are presented in a section for each identified GaAs nanowire facet and one section for the wurtzite-zincblende transition.

The morphology of the nanowires will be presented, starting with the {110} zincblende facet on the top part of the hexagonal cross section nanowires. It is followed by images of the {11-20} facet and the transition between those two facets. The {10-10} type side facets identified for the wurtzite bottom part of the studied nanowire sample are then presented.

Each image or set of images is followed by an interpretation and discussion of what is believed to be observed. It should be noted that most of the presented images are taken with negative applied voltage, meaning that As atoms that are imaged. The growth direction of the nanowires is marked in the images, pointing towards the gold particle.

4.1 {110} Zincblende facet

The {110} facet were expected to be seen for the zincblende structure. In structure 'models' of the facet, presented in section 2.3.3, rows of As and Ga lying with an angle of about 35° with respect to the nanowire growth direction are expected. Depending on if the applied tunneling voltage is positive or negative, either a filled state image of As atoms or an empty state image of Ga atoms are obtained according to present understanding. Most images were taken with a negative sample bias, resulting in imaging of group V atoms.

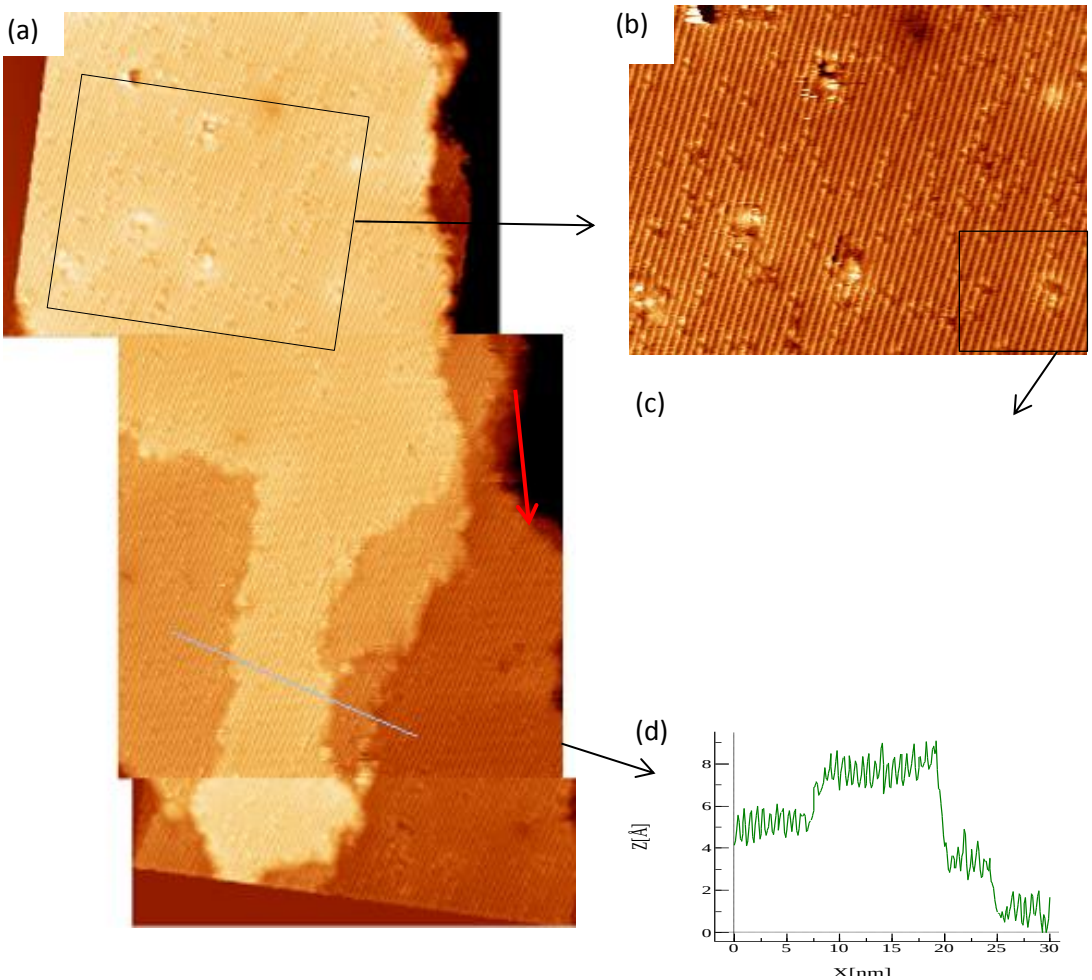

Figure 4.1: (a) Three images of the {110} facet put together afterwards showing the surface structure. The individual images are taken with an applied voltage of $V_T = -2.5$ V and a tunneling current $I_T = 150$ pA. The combined image has a length of 106 nm and the top image is located about 40 nm above the Zb-Wz transition. The red arrow shows the growth direction. (b) Image of the size 35x27 nm^2 zoomed in at the top part of (a) showing a high density of point defects. A 25 nm long line profile is taken perpendicular to the rows indicated by the gray line. (c) 10x10 nm^2 zoom in showing the observed defects (d) The 30 nm long line profile from (a) taken over several of the observed step.

Figure 4.1 (a) represents a typical view of the {110} facet, with a width of about 60-80nm. The surface morphology seen in the last mentioned figure were commonly observed for the {110} surface facet with rows lying diagonal to the growth direction. Several layers of the

surface are visible in a region of the same figure, which appears to be a general pattern. The uppermost layer is seen to be the least wide one, still covering the whole facet. The edges of the terraces are seen to be wavy, rather than straight. The terraces seem to be disrupted by steps in several different directions. It should be noted that the group of terraces all end in a step of a height of several combined steps, lying in the same direction, roughly along the direction of the rows. This morphology is also seen for the {110} facet shown in figure 4.2 (a) below. Judging from the line profile taken over the steps, shown in figure 4.1 (d), the step heights are 2-2.3 Å or multiples of that. This clearly indicates that atomic steps are seen on the facet. No stacking faults are observed in the zincblende crystal structure as seen on the {110} facet, indicating high quality nanowire growth as specified be the manufacturers. [7]

At least one type of point defect is found on the surface, possibly several depending on the interpretation of images of the defects taken with different voltage and/or tunneling current. A rather high density of small dark point defects of a size below a nanometer, are showed in the smaller scale images of figure 4.1 (b) and (c).The defects show slightly different appearance under different scanning parameters but are seen on nanowires in several nanowires of the sample on the discussed facet. The density is determined to be of the order $10^{13}\mathrm{cm}^{-2}$ although more statistics is required to make an accurate claim. Additionally, several larger bright spots can be seen and also a depression area of several nanometers. The size of the small dark defects is measured to be about 5 Ångström, and the measured height decrease at the size of the defects is around 1-1.5 Å, corresponding to the corrugation measured for the surface in the same image. Another interesting observation is the position of the imaged defect and the fact that the atomic states next to the defects appear brighter. A measurement of these neighbouring states shows that they are elevations of up to 0,5 Å.

The size, depth and density of the defects indicate that it is mono vacancies that can be seen. The size of the 'hole' situated in As rows agrees with the dimensions of one dangling bond. The localized hole arises from a missing atom which had been connected to the dangling bond. [24] An explanation to the brighter neighboring states is presented in previous studies of vacancies of this surface. It is there concluded that these are increases in the occupied dangling bonds due to a negatively charged Ga vacancy. [24]

One example of the different appearance of the defects is presented below. These images are taken with the same voltage as that of figure 4.1 but with considerably lower tunneling current.

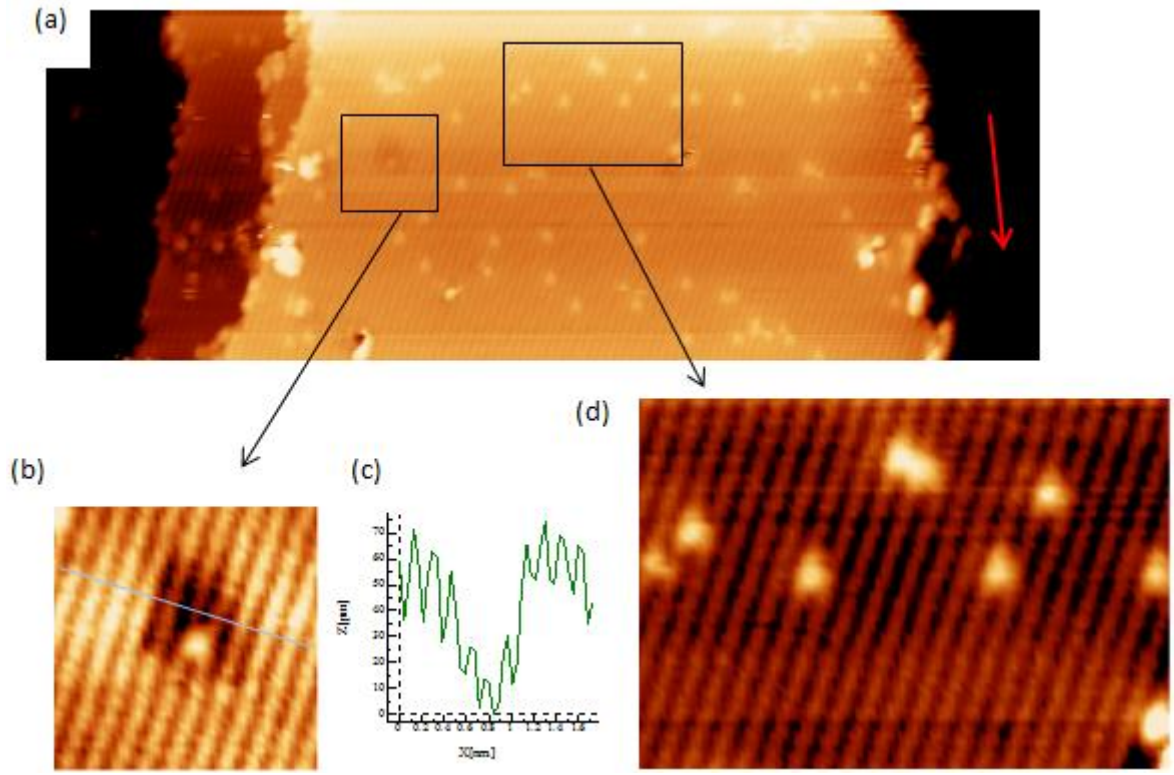

Figure 4.2: (a) 80x28.3 nm^2 image of the {110} facet showing the surface morphology of wide terraces and several atomic layers with steps along the diagonal. The images are taken with an applied voltage of $V_T = -2.5$ V and a tunneling current $I_T = 80$ pA. The nanowire growth direction is indicated by the red arrow. (b) 7x7 nm^2 zoom on a region with defects together with an added line profile perpendicular to the atomic rows. (c) Line profile corresponding to the line in (b) showing sub-Ångström height variations. (d) 14x10 nm^2 zoom on the bright spots seen in image (a).

Figure 4.2 again shows the {110} facet with high enough resolution to resolve atomic rows and individual defects. The density of this type of point defect is in the same order of magnitude as the ones seen in figure 4.1 (b) and (c) which points towards that it is the same type of defect. The size and apparent height of the spots suggests that the bright spots might be attributed to electronic effects. A difference, possible attributed to the difference in tunneling current, is the fact that no clear hole can be seen in the middle of the bright spots. It is also plausible that Measurements of the size of the bright spots show that they are about 1 nm wide and lay about 0.5 Å above rest of the surface; this agrees well with the measurements of the elevations of the states next to the 'holes' obtained from figure 4.1 (c). It is noted that the spots are located in-between two atomic rows rather than in the rows themselves. This is another type of defect due to the different position in relation to the lattice.

In figure 4.2 (b) another feature can be seen. A darker area spread out over several square nanometers, corresponding to a couple of atomic rows. The line profile in (c) shows that the height decreases with about 0.5 Å across this area. This means that it can be attributed to electronic effects of a defect and not due to missing atom itself. These depressions are voltage dependent and can result from charged vacancies inducing a local band bending.

From figure 4.2 d), a row separation of 6.05 Å is measured for the atomic structure. The row separation is from models of the {110} facet, expected to be equal to the lattice constant of the zincblende structure. This distance is measured accurately to 5.65 Å in previous studies of the surface. [26] The agreement is reasonably good with a discrepancy of less than 10%. The disagreement is probably due to non-optimal STM calibration and Piezo electric drift.

To determine the atomic spacing more accurately, the drift towards or away from the scanning direction is taken into account. This is done by averaging over measurements of the row separation in several pictures of the {110} facet, taken with the roughly same applied voltage and currents but with different scanning direction. Such measurements can be obtained from the images shown below.

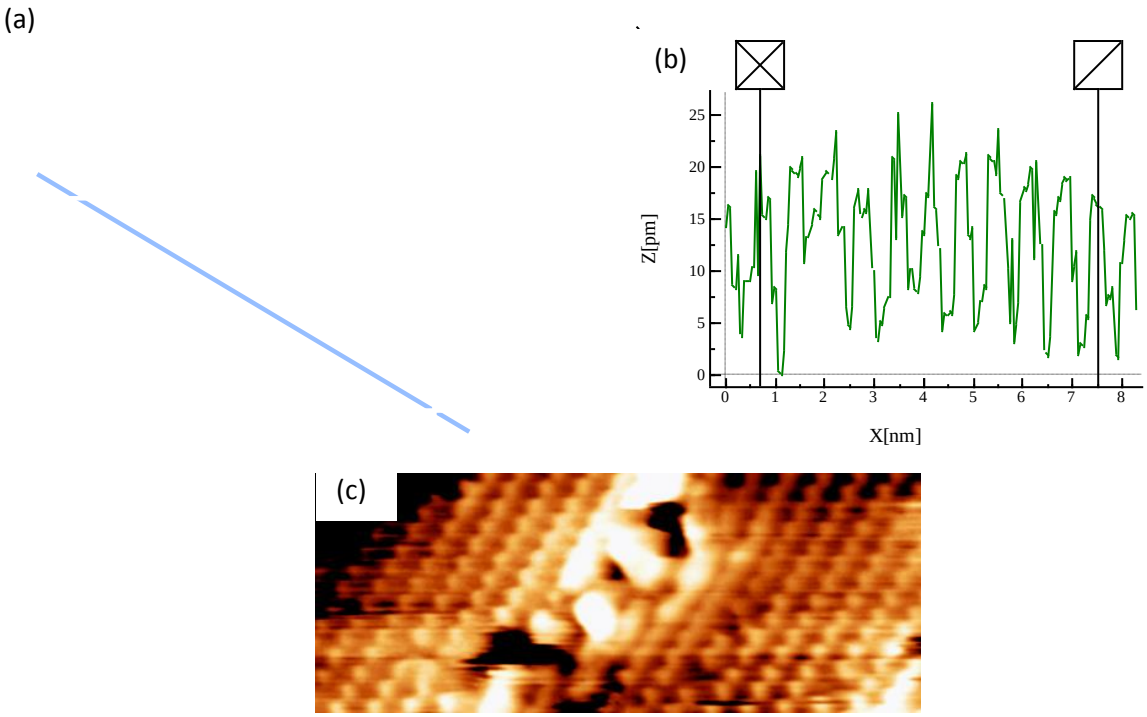

Figure 4.3: (a) 10x7 nm^2 image with atomic resolution obtained with an applied voltage of $V_T = -2.5\ V$ and a tunneling current $I_T = 100\ pA$ with upward scanning direction. Distance between atoms along the rows is measured to 5.2-5.4 Å by averaged over 10 distances. (b) Line profile from which a row separation of 6.7-6.9Å where obtained by averaging over 10 rows. (c) 12.5x5 nm^2 image obtained with an applied voltage of $V_T = -3.0\ V$ and a tunneling current $I_T = 100\ pA$ and downward scanning direction. Distance between atoms along the rows is measured to 4.3-4.5 Å and the distance between rows is measured to 6.0-6.3 Å by averaging over 5 atom separations.

The values presented for the two images clearly demonstrates the effects of drift in the images resulting in stretched or compressed distances depending on the scanning direction. The ratio between the distance between rows compared to the atom-atom distance along rows is 0.75-0.8 using the values obtained from image 4.3 (a) and 0.7-0.75 for measurements done with figure 4.3 (c). The predicted ratio from the model of the {110} zincblende plane is $\frac{\sqrt{2}}{2} = 0.707$, which means that the agreement is reasonable with a discrepancy of around 10% or less.

4.2 {11-20} Wurtzite facet

For the wurtzite crystal structure adopted by the lower part of the nanowires, {10-10} and {11-20} top facets were observed. The [11-20} facet were identified by zigzag rows appearing in the direction of the nanowire as stated earlier.

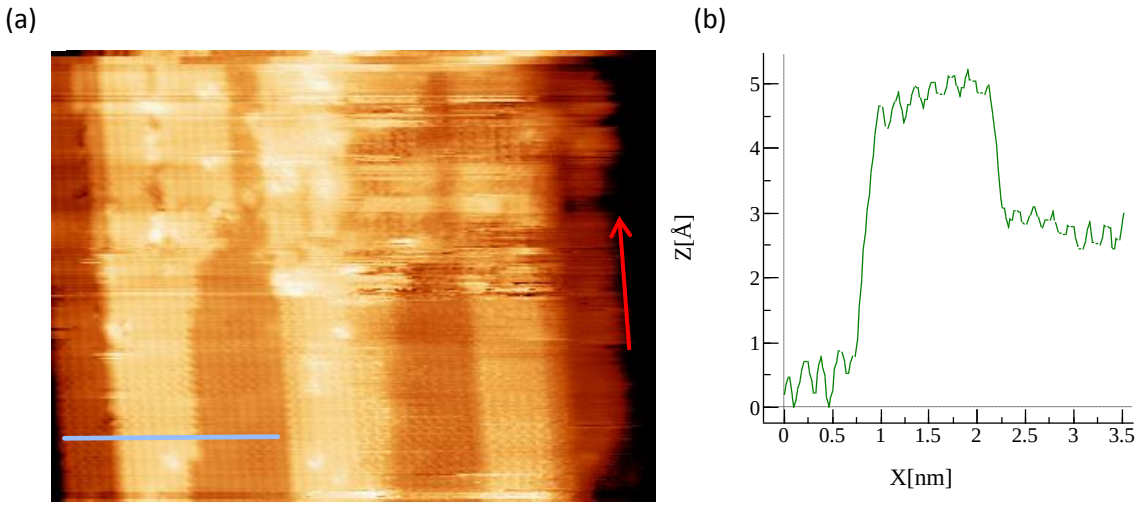

Figure 4.4: (a) Image of the size: 40x30 nm^2 showing the main structural features of the wurtzite {11-20} facet. These include sharp facet edges and a finger-like overgrowth directed downwards along the nanowire. The parameters used when taking the image were $V_T = -3.0$ V and $I_T = 100$ pA. The red arrow points towards the top of the nanowire. (b) Line profile corresponding to the line in (a) showing the height of the overgrowth.

As seen from figure 4.4 (a), the morphology of the {11-20} wurtzite facet differs from the zincblende facets. The size of the {11-20} facets were observed to be about 40-50 nm wide, which is considerably less than the {110} facets. The expected zigzag rows along the growth direction are seen. The surface morphology is dominated by finger-like overgrowth of stripes covering the uppermost layer. The width distributions of the stripes are anything from a single atomic row up to about 10-15 nm. They occur preferably along the direction of the nanowire. This is in sharp contrast to the morphology of the {110} facet where different layers covered the whole facet without any sharp and preferred edges. The stripes lay one or two atomic steps above the rest of the surface as is seen in the line profile in figure 4.4 (b). The width of the overgrowth is observed on several nanowires, to decrease further away from the transition to zincblende as is seen in Figure 4.4. The image of this figure also goes to show the undesired effect of an unstable tip, giving rise to the horizontal noisy scan-lines.

On the {11-20} facet, almost no point defects of the sort observed on the {110} surface were found on the surface. Rows of what appears to be missing atoms were however observed, especially on the overgrowth terraces, but also on the lower layers, with length of up to 10 nm. Two such cases can be seen with some effort in the non- optimal image of figure 4.4 (a), in the top part of the image.

(a)

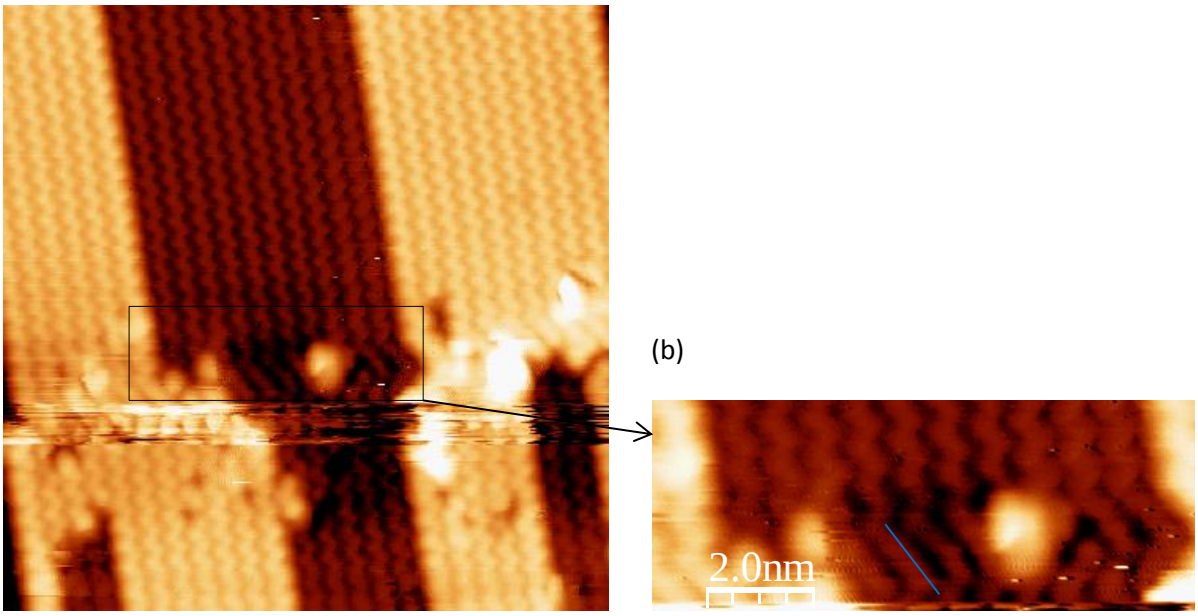

Figure 4.5: (a) {11-20} atomic zig-zag rows and a stacking fault in the wurtzite crystal structure. The image size is 20x20 nm^2. The image is recorded using a voltage of $V_T = -2.5V$ and a tunneling current of $100\ pA$. (b) Close up on a stacking fault resulting in a single segment of zincblende, emphasized by the blue line.

Figure 4.5 represents a typical view of the {11-20} wurtzite facet. The finger-like overgrowth can be seen in the zoomed-in image of figure 4.5 (a). The top layer has sharp edges ending along one atomic zig-zag row. As mentioned in the theory section, a single misplacement in the Wz gives rise to a single Zb segment. The crystal defect is measured to be about 2 nm wide, in agreement with the size of one stacking fault as measured for InAs in previous studies. [23] It can therefore be assumed to be a single Zb sequence.

The stacking fault is seen to consist of zincblende stacking before going back to the wurtzite stacking sequence ABAB again. The appearance of a stacking fault seems to displace and change the structure of the overgrowth on the other side of it. This has been observed more than once, but it's not concluded that it's a general feature. The density of stacking fault in the wurtzite crystal structure away from the immediate vincity of the transition between the wurtzite and zincblende structure is below 20 μm^{-1} as specified by the manufacturers. [7]

Shown in the image are also a few dark spots of the size of individual atoms. These spots have a depth of about 1-1.5Å, which point towards missing atom(s) in the first layer. The position of what appear to be mono vacancies, agrees with the zig-zag placement of the imaged Arsenic atoms. It is therefore assumed to be As vacancies. It can be noted that these defects only seem to occur near the stacking fault with a Zb crystal segment. One idea is that it is more energetically favorable for them to occur close to the crystal defect.

Looking closer at the atomic spacing's of the {11-20} plane, one sees two near quadratic patterns overlapping and creating the zigzag rows. This is better seen in the high resolution on the next page.

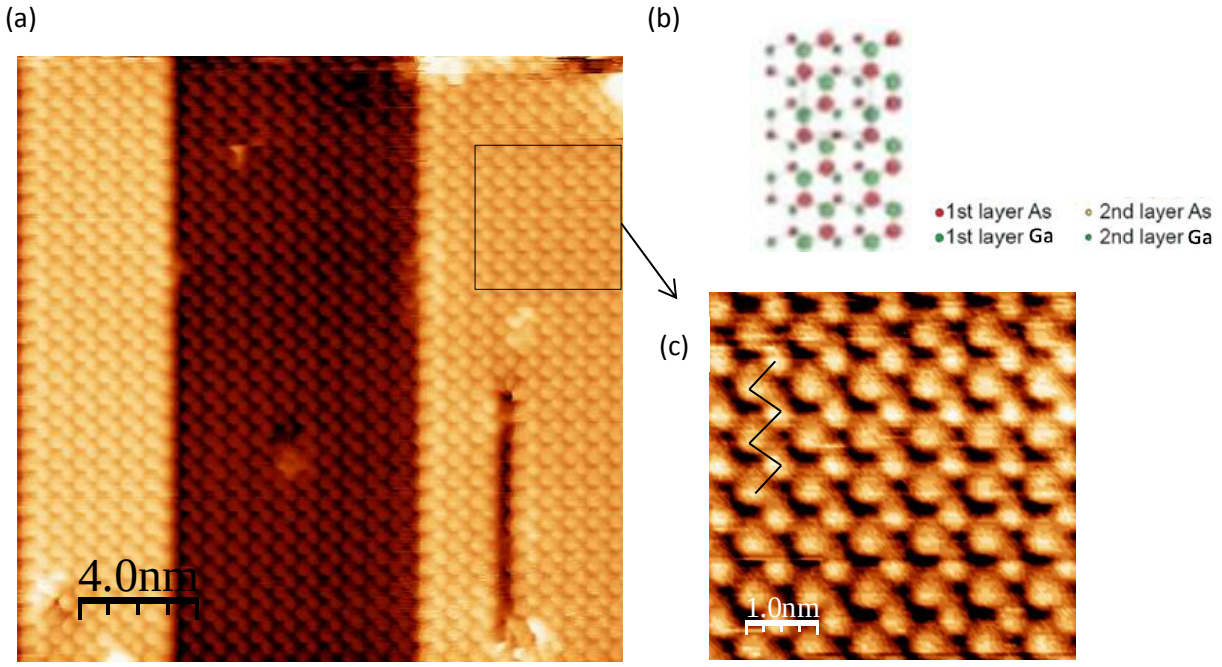

Figure 4.6: (a) 20x20 nm^2 image showing {11-20} top facet with atomic zigzag rows and a row of missing atoms in the lower right part. The image is taken with a voltage of -1.9 V and a current of 100 pA with an upward scanning direction. (b) Atomic model of the first two layers of the {11-20} facet. [8] (c) A blow-up of the size 5x5 nm, showing atoms of different apparent size, each forming a near-square pattern. The zig-zag rows are here indicated by a black line. The distance between two atoms along the direction of the nanowire is measured to 6.9-7.0 Å and parallel to the nanowire growth direction: 7.5-7.6 Å.

The measured distances show a ratio of 1.05-1.1 between the atom separations parallel to the nanowire direction as compared to the separation in the perpendicular direction. Similar measurements done in an image taken with same voltage and current settings at the same occasion but with opposite scanning direction yields the same values of 6.9-7.0 Å respective 7.5-7.7 Å, indicating an absence of a drift noted in previous images. The measured distance ratio of the near-square pattern is in reasonable agreement with the atomic structure as described by the model.

Interestingly, every other atom in the vertical zigzag rows appears to be larger than the rest. The reason or explanation to this is uncertain. The height difference between these were compared by measuring the atom height of all atoms in one row parallel to the nanowire direction and comparing with the next and then averaged over several such rows. The atoms appearing larger were measured to be 0.1-0.15Å above the others, the large relative uncertainties involved however makes it hard to conclude anything.

A feature mentioned earlier can be seen in figure 4.6 (a). It is the 10 nm long vertical row with a width of an atomic spacing. The depth of the feature is measured to around 2Å, which agrees with the size of an atomic step seen in the image. This again indicates that such rows are due to a row of missing As atoms in the first layer. Such rows were observed at several occasions on the {11-20} facet. Figure 4.7 (a) on the next page is one such image.

(a)

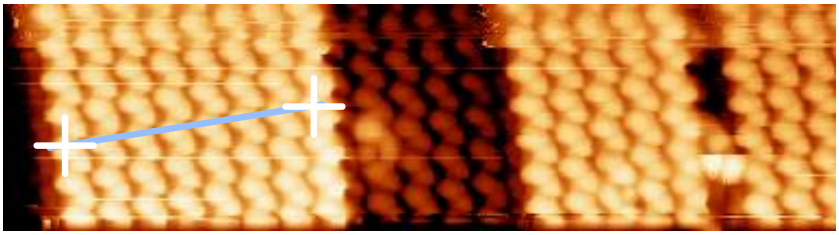

(b)

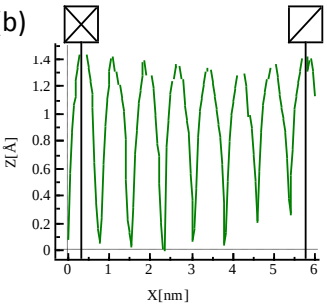

Figure 4.7: (a) 18x5 nm^2 image showing a zoomed in image of the atomic zigzag-rows measured to have atomic spacing's of 7.6-7.8 Å perpendicular to the growth direction and 7.3-7.4 Å parallel to it. The image is taken with a voltage of -2.5 V and a current of 100 pA with an upward scanning direction. (b) Line profile showing a corrugation of 1-1.5Å when measuring atomic spacing perpendicular to the [0001] growth direction

The ratio between atomic spacing parallel and perpendicular to the NW is again measured to around 1.05, while with distances are scaled up a factor of 1.05 owing to thermal drift or piezo nonlinearity.
The high resolution image in figure 4.7 (a) shows another atomic scale feature along with the larger scale features mentioned before. In the row of vacancies and also near the middle of the image, one can see atoms that appear to be incorrectly positioned. One explanation for these could be that they are intersituated atoms.

4.3 The transition {110} - {11-20}

The transition between the wurtzite and zincblende structure is observed as a sharp transition of the wide {110} facet with atomic rows diagonal to the direction of the nanowire to a smaller {11-20} facet with zigzag rows along the nanowire. The transition is often observed together with stacking faults or mixed crystal structure in a region around it.

(a)

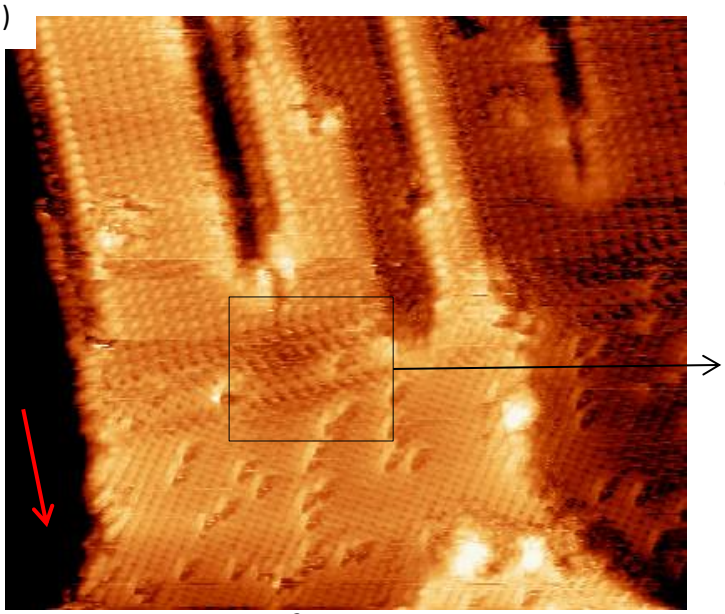

(b)

Figure 4.8: (a) 35x30.6 nm^2 image showing the transition between the {110} facet seen in the bottom of the image and the {11-20} facet seen in upper part. The parameters used when taking the image were V_T=-2.5V and I_T=150 pA. (b) 10x10 nm^2 close up showing the area where the transition occurs. Red arrow notes the growth direction.

The transition is accompanied with one or multiple atomic bilayer misplacements in the observations made of the transition. These observations are done for different nanowires of the same sample. These crystal defects at the transition typically extend over a 2-5 nm region, with atoms laying in the direction seen in figure 4.8 (b). The resolution is not high enough to determine the atomic spacing for the rows in (b).

Figure 4.8 (a) supports the model expecting a diameter increase when going from the {11-20} facet of the wurtzite structure to the zincblende {110} as can be hinted by the bending occurring in the lower left part. No height change is observed to occur at the interface between the two crystal structures.

The rows on the zincblende structure lie with an angle of approximately 35° to the direction of the {11-20} rows which extend in the direction of the nanowire. The rows of atoms seen in figure 4.8 (b) show an angle of approximately -30° with respect to the nanowire direction. This agrees with the observations of the previously discussed stacking fault in the wurtzite crystal structure.

The overgrowth of the {11-20} facet starts from the transition where the upper layers of {110} split up into several finger-like structures continuing down along the wurtzite part of the nanowires, where it becomes smaller and smaller.

The defects on the {110} facet can again be seen in figure 4.8 (a).The appearance of both the atomic structure of the {11-20} surface and the defects on the {110} facet look a bit strange. This is probably an artifact of the tip used when taking the image.

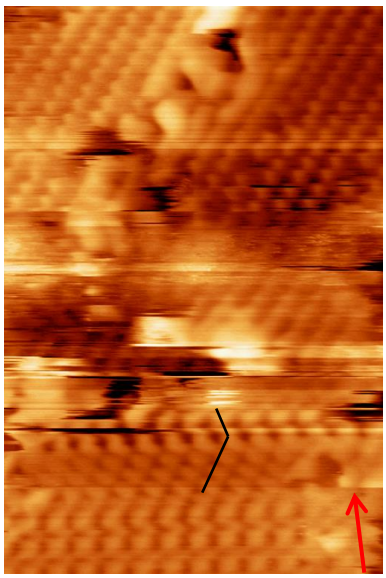

Figure 4.9: 10x15 nm^2 zoomed in image of the area of the transition {110}-{11-20} with a crystal defect indicated by the black lines. The image is recorded with an applied sample bias of V_T=-3.0V and a tunneling current of 100 pA. The red arrow points approximately in the nanowire growth direction. The image also demonstrates the effects of small tip changes often seen at the transition, resulting in a blurry region.

In Figure 4.9 the distance between atoms along the {110} rows is measured to 4.3-4.5Å and the distance between rows is measured to 6.0-6.3 Å by averaging over 5 atom separations. The lattice constant of the GaAs {110} zincblende surface is reported to be 5.65 Å. [26] The lattice constant of the zincblende structure corresponds to the atomic row separation which was measured to 6.0-6.3 Å. This can be used to calibrate the measurement performed on the {11-20} atomic structure of the lower part of the image. The non-calibrated measured distances are 7.4-7.5 Å perpendicular to the NW direction and 6.9-7.1 Å parallel to the NW. Using the calibration the values become 6.7-6.9 Å respective 6.3-6.5 Å.

4.4 {10-10} Wurtzite facet

The {10-10} wurtzite facet was most often observed as side facets, which were hard to image. When it showed up as a top facet it was seen to be 50-70 nm wide and showed a surface morphology of multiple steps occurring every 20-50 nm together with an overgrowth structure. This facet was harder to image with atomic resolution, but showed atomic rows perpendicular to the nanowire as expected for the {10-10} wurtzite structure according to the model from section 2.3.3 about the nanowire surfaces

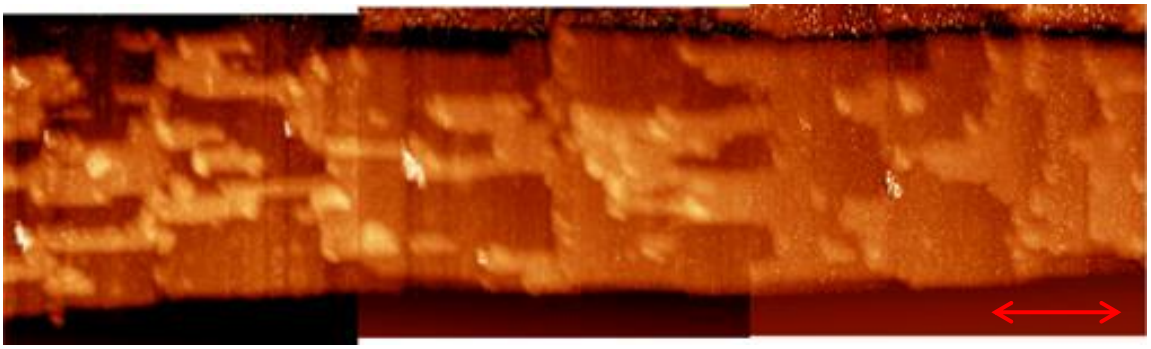

Figure 4.10 Three images put together showing 260 nm of the Wurtzite {10-10} morphology. The height of each image is 75 nm and they are recorded with a sample bias of -2.5 V and with a 60 pA tunneling current. The growth direction is indicated the arrow.

The {10-10} type facets show a morphology which differs significantly from the zincblende morphology and also from that of the {11-20} wurtzite facet. It is observed that a step structure is present at the wurtzite part of the nanowire. Each step ends perpendicular to the growth direction with the upper layer partly continuing onto the next step. This structure is slightly different from that of the {11-20} facet, changing direction and size in a less predictable manner. The frequency with which new steps appear seems to increase when going from one end of the nanowire to the other.

Looking closer at the overgrowth structure and the steps occurring along the nanowire one can see that the height of the overgrowth above the rest of the nanowire surface facet is about the same along the wire, corresponding to an atomic step.

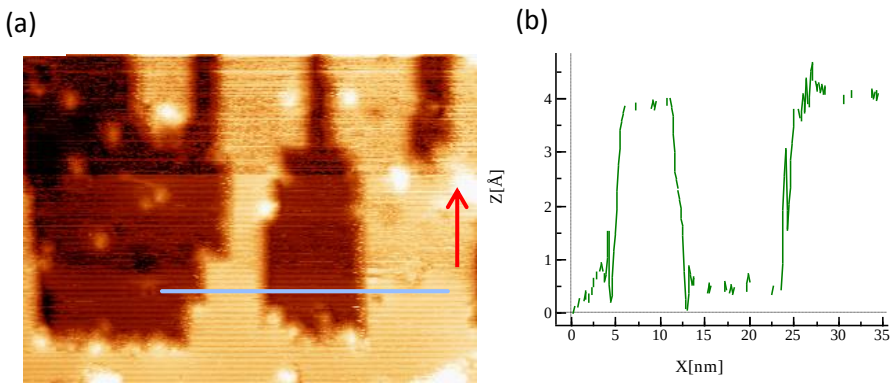

Figure 4.11: (a) 55x40 nm^2 image showing the overgrowth structure of the {10-10} nanowire facet. (b) A 35nm long line profile shows that the height of the structure height is about 3.5 Å. The red arrow indicates the growth direction.

The height of one overgrowth layer is about 3.5 Å based on the fact that no smaller height differences of two layers have been observed on the {10-10} facet. This means that the height of one layer of {10-10} layer is much larger than for the other two studied facet types where the step size was measured to about 2 Å. The width of the terraces typically varies a lot, ranging from 5 to 25 nm measured perpendicular to the nanowire growth direction. As with the overgrowth on the {11-20} facet it is directed along the nanowire. The width changes several times over a short length, which is in contrast to the structure seen in figure 4.4 (a) and 4.6 (a).

The {10-10} facet showed a low density of point defects just like the other wurtzite surface. One type of defects can be identified as bright spots in figure 4.11 (a). The dimensions of these defects are of the order 1x1 nm^2 and shows a height of 1.5-2 Å above the rest of the surface. Secondly, depression regions of similar size are located on the surface. These are the result of electronic effects, possible due to the charge of a defect.

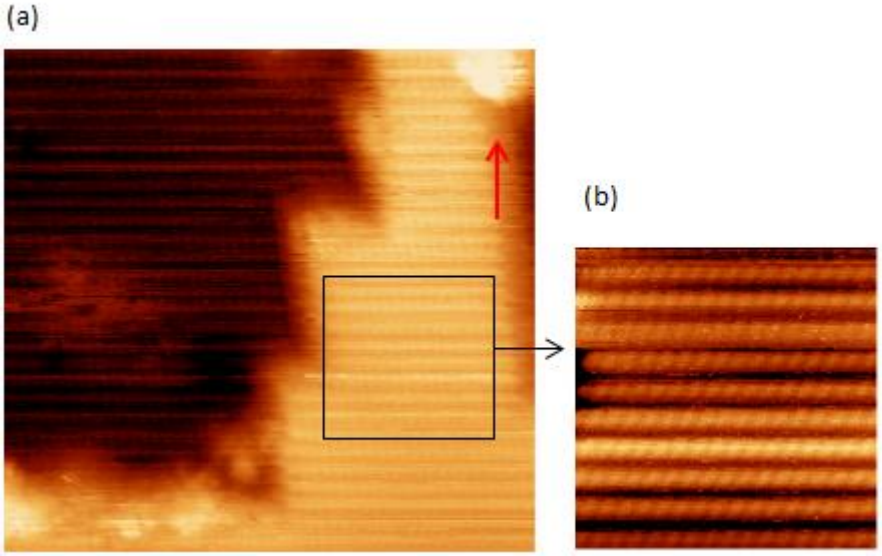

Figure 4.12 (a) Atomic rows perpendicular to the nanowire growth direction in a 20x19 nm^2 image taken at V_T=-2.5 V, I_T=150 pA. The red arrow points in the nanowire direction (b) Image taken with atomic resolution showing a 7x7 nm^2 area with atomic rows as well as individual atoms in the rows.

On the {10-10} facet the separation between the rows orthogonal to the nanowire is large compared to the interatomic distance of atoms in the rows as can be seen in figure 4.12 (a). The atomic spacing between atoms in the rows is measured to 4.3-4.4 Å averaged over 13 spacings. The separation between two rows is determined to 6.9-7.1 Å by averaging over 10 rows. The atomic spacings of the {10-10} plane is from models expected to be equal to the lattice parameters "a" and "c" for the hexagonal wurtzite structure. A ratio $\frac{c}{a} = 1.6 \pm 0.1$ is obtained using the values stated above. This is in excellent agreement with the predicted ratio of c/a=$\sqrt{8/3} \approx 1.633$, stated before.

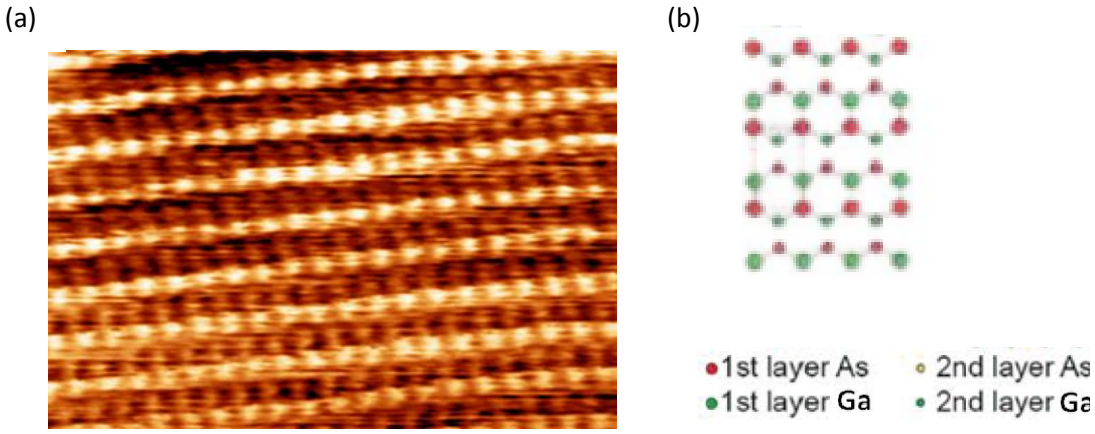

Figure 4.13: (a) Approximately 6x4 nm^2 filtered image showing the atomic structure of the {10-10} facet, taken at an applied voltage of V_T=-=-1.6V and current I_T==150 pA. (b) Model of first two layers of the {10-10} facet.

Figure 4.13 (a) has atomic resolution of the {10-10}, clearly showing rows of individual atoms. By comparing to the model one can say that the As atoms of the first layer are here observed together with atoms from the second layer. Although the image is observed to have some drift, the best agreement of the observed 2nd layer atoms is obtained by assuming it to be As atoms. This conclusion is based on that their location near the middle of the rectangular structure of the As atoms of the first layer. Measurements of the height difference support this conclusion.

4.5 (111)B Zincblende facet

The least commonly observed facet was expected triangularly shaped facet. It was identified to be the (111)B facet for the zincblende part of the nanowires. The facet was found to be located at the transition from wurtzite to zincblende structure connecting the wurtzite {10-10} top facet to zincblende {110} side facets. The (111}B facet is thought to compensate for a slight increase in the diameter of the hexagonal cross section nanowires for the Zb part as well as a rotation of facets of about $30°$ occurring at the Zb-Wz transition. [7]

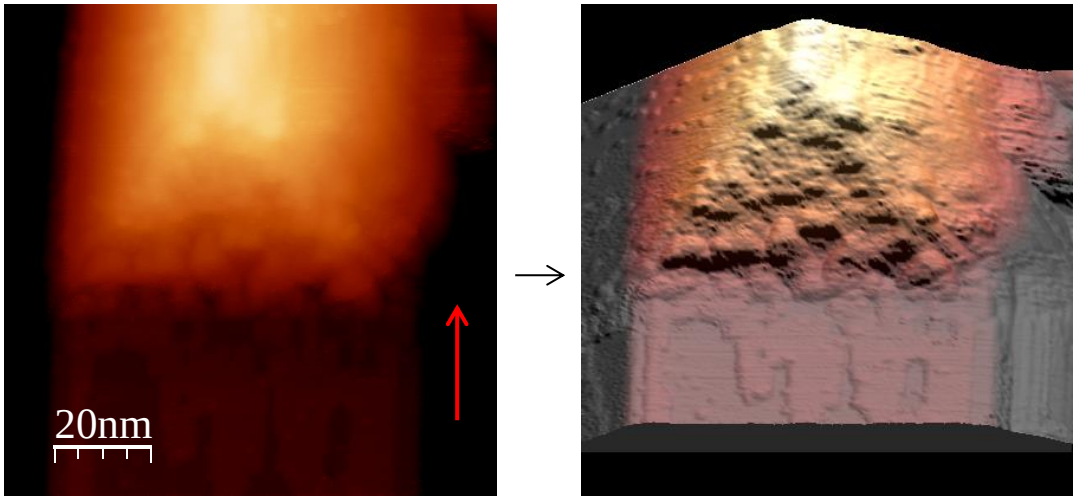

Figure 4.14 (a) 100x100 nm^2 image showing the transition from wurtzite (bottom part) to zincblende (upper part) with a triangular (111)B facet. The arrow points towards the gold particle at the end of the nanowire. (b) Shows a 3D model of the area imaged in (a).

The shape is determined to be close to that of an equilateral triangle with a side of about 60 nm, although the edges of the facet are not totally well defined. The surface of the (111)B facet is observed to be rougher than the other facets showing several bumps 5-10 nm in size. These are located primarily in the lower parts of the (111)B facet but also around the edges of the facet and onto the {110} facet. The rougher surface could be a response to the heating of the nanowire during the cleaning process or just a growth structure inherent to the nanowires.

Going from the base of the triangular facet at the Zb-Wz interface to the upper corner of the facet, a height increase of 15 ± 1 nm occurs over a vertical length of 45 ± 5 nm. This results in that the (111)B facet lies with an angle of $18° \pm 3°$ relative to the facet in the lower part of figure 4.14.

In figure 4.14 (a) one can also see that the overgrowth structure seen on the {10-10} facet continues from the transition region of the (111)B facet downwards.

5 Conclusions and summary

Scanning tunneling microscopy and spectroscopy have been applied in this bachelor thesis, to take high resolution images of GaAs Wz-Zb heterostructure nanowires. The goal of the study was to characterize the nanowire surfaces of the studied nanowires. Successful experimental preparation and nanowire cleaning has made it possible to obtain a large set of data. Before the studies of the GaAs nanowires had begun, it was not known how hard it would be to clean them from oxides and to image the different facets. The work in this thesis indicates that the atomic hydrogen cleaning worked well on GaAs nanowire surfaces at an annealing temperature of about 500°C, hydrogen pressure of $2\cdot 10^{-6}$ mbar and with an annealing time of 20 minutes.

The morphology of the GaAs nanowires facets were investigated after identification, made possible by the differing atomic structure of the various nanowire facets. Identification of both {110} top facets and a triangular (111)B facet were possible for the zincblende top part of the nanowires. {10-10} and {11-20} wurtzite facets were identified on the lower part of the nanowire heterostructure owing to their different atomic structure.

The zincblende top part showed 60-80 nm wide {110} facets. The morphology of the {110} facet is dominated by wide terraces covering the whole facets ending in atomic steps with varying directions roughly along the direction of the atomic rows, diagonal to the nanowire growth direction. The facet is observed to have at least one type of point defects distributed rather homogeneously over the whole surface. These are thought to be As mono vacancies in the first atomic layer. Stacking faults and mixed crystal structure were absent from the zincblende top part of the nanowires.

The {110} Zb facet is connected to a {11-20} facet, which is observed to be much thinner. The {11-20} facet is observed to have a finger-like overgrowth structure, up to 10-15 nm wide. The overgrowth is directed downward along the nanowire. A decrease in the width of this structure occurs when moving away from the Zb-Wz transition. A change to the otherwise sharp straight edges of the structure occurs at stacking faults in the wurtzite structure.

The transition from Zb to Wz crystal structure, which occurs after a fraction of the NW length, is also imaged. The transition from Zb to Wz crystal structure is observed to be accompanied with a region of crystal defects about 2-5 nm wide including stacking faults. From the transition region between the {110} and {11-20} facet, an overgrowth structure is observed to start from the transition and continue onto the {11-20} facet. The {11-20} facet is observed to have rows of Arsenic vacancies, but no point defects of the type seen on the {110} facet was observed for this facet.

From observations made of the {10-10} facet, its surface morphology can be said to consist of sharp atomic steps occurring every 10-50 nm, perpendicular to the nanowire growth direction. From each step between two atomic layers, a structure continues and ends further down along the nanowire on the lower layer. This structure of atomic steps parallel to the nanowire covers a large part of the {10-10} wurtzite part nanowire. From atomic scale images, both the As atoms in the first and second layer could be matched to the model of the atomic structure. The facet is observed to be almost free of point defects.

Stacking faults resulting in Zb sequences are observed in the wurtzite crystal structure where more point defects are seen to be located. The density of stacking faults is lower than the specification by the manufacturers of 20 μm^{-1}, indicating high quality nanowires.

A triangular (111)B type facet was observed at the zincblende Zb-Wz transition. The triangular facet was measured to have sides about 60 nm long and its upper edge was at a height of 15 nm above the {10-10} surface on the Wz part of the nanowire. The facet connected the wurtzite {10-10} top facet to zincblende {110} side facets. The surface of this facet was rougher than the other surfaces, showing several bumps of sizes ranging from a few nanometers up to 5-10 nm. It was however only observed once with reasonable image quality.

6 Outlook

The present work is merely a beginning of the scanning probe microscopy studies of GaAs Zb-Wz heterostructure nanowires. Continued studies needs to be performed on clean GaAs nanowires in order to obtain the statistics to fully map out the surface morphology. Particularly the wurtzite facets, needs to be further investigated with STM since their nanowire surface morphology is not as well known.

In this thesis preliminary STS measurements were performed on the nanowires. It proved to work, yielding a band gap expected for GaAs surfaces, when taking band bending into account. Continued studies of the electronic properties of the nanowire heterostructure are needed, to determine the influence of the observed stacking faults and point defects. The structure of the edges of the hexagonal nanowires is not known well, and attempts to determine these would surely be of importance for the properties of the structure.

The performed measurements have resulted in a large data set in great need of further interpretation. of the source of the observed point defects and crystal defects. Theoretical models which can provide explanations of the observed surface morphology, and its relation to the growth process are of great interest. That would lead to better control of the electronic properties, when growing the nanowires.

Several different approaches to further studies can also be imagined. An interesting idea would be to study the GaAs nanowire surface facets in relation to adsorption. This would presumably yield information about the performance of the structures under less artificial conditions. When the basic properties of the nanowire heterostructures are known to some degree, a next step would be to investigate them in operation with contacts and applied bias to do measurements on their conductivity.

References

[1] MLA style: "Press Release: The 1986 Nobel Prize in Physics". Nobelprize.org. 14 May 2012 http://www.nobelprize.org/nobel_prizes/physics/laureates/1986/press.html

[2] H. Xu, “Fabrication and electrical/optical characterization of bulk gallium nitride-based Schottky diodes”, http://www.grin.com/en/doc/234203/fabrication-and-electrical-optical-characterization-of-bulk-gallium-nitride-based , 17 Jun 2012

[3] H. Timmers, ”*Functionality from Electronic Materials*”, http://www.pems.adfa.edu.au/~s9471553/level1/Teaching/ElectronicProperties/Functionality.html, 17 Jun 2012

[4] E. Hilner, “Characterization of surfaces relevant to nanotechnology”, Lund University ISBN: 978-91-628-7965-5, pp. 33-40, Nov 2009.

[5] L. J. Lauhon, Mark S. Gudiksen and Charles M. Lieber, “Semiconductor nanowire heterostructures”, *Phil. Trans. R. Soc. London, Ser. A*, vol. 362, pp. 1247-1260, Apr2004.

[6] K. A. Elamrawi, *et al*, “Atomic hydrogen cleaning of InP(100) for preparation of a negative electron affinity photocathode”, *Journal of Applied Physics*, vol. 84, pp. 4568-4572, Oct 15 1998

[7] S. Lehmann, *et al*, “High crystal quality wurtzite-zincblende heterostructures in MOVPE- grown GaAs nanowires”, manuscript to be published, pp. 1-8, 2012.

[8] M. Hjort, “Surface studies of III-V nanowires”, Lund University ISBN: 978-91-7473-313-6, pp. 3-16, 2012.

[9] E. Hilner, “Characterization of surfaces relevant to nanotechnology”, Lund University ISBN: 978-91-628-7965-5, pp. 18-20 , Nov 2009

[10] G. Attard and C. Bartes, “Surfaces”, *Oxford science press*, pp. 57-60, 1998.

[11] R. M. Feenstra, “Scanning tunneling spectroscopy”, *Surface Science,* vol. 299-300 ,pp. 965-979, 1994

[12] P. Matensson and R.M Feenstra, “Voltage-Dependent Imaging of Antimony on the Gaas(110) Surface”, Journal of Microscopy-Oxford, vol. 152, pp. 761-769, Dec 1988.

[13] Dawn Bonnell (ed.), “Scanning Probe Microscopy and Spectroscopy: Theory, Techniques and Applications”, 2. edition ed., John Wiley & Sons, 1 , pp. 60-67, 2001.

[14] “Genera properties of ZnO”, http://media.wiley.com/product_data/excerpt/34/35274081/3527408134.pdf, 17 Jun 2012

[15] J. Johansson B. A. Wacaser, K. A. Dick, and W. Seifert, “Growth related aspects of epitaxial nanowires,” *Nanotechnology*, vol. 17, pp. 355-361, 2006.

[16] G. R. Bell, N. S. Kaijaks, R. J. Dixon, and C. F. McConville, “Atomic hydrogen cleaning of polar III-V semiconductor surfaces”, *surface science*, vol. 401, 125, 1998.

[17] S. Pröller, “Scanning Probe Microscopy of InAs/InP Nanowires”, Bachelor Thesis : Lund University, pp.3-12, Apr 19 2011.

[18] E. Erdogan, “Bulk oxide growth on Rh(111) surface”, Master Thesis: Lund University ,pp. 35-39, May-2011.

[19] P. Caroff, *et al*. , ”Crystal Phases in III-V Nanowires: From Random Towards Engineered Polypism”, *Ieee Journal of Selected Topics in Quantum Electronics*, vol. 17, pp. 829-846, Jul-Aug 2011.

[20] J. Frenken, “Principle of Scanning Probe Microscopy, http://www.physics.leidenuniv.nl/sections/cm/ip/group/Principle_of_SPM.htm, Interface Physics Group, 21 Jun 2012
[21] E. Hilner, U. Håkanson, L. E. Fröberg, M. Karlsson, P. Kratzer, E. Lundgren, L. Samuelson, A. Mikkelsen, “Direct Atomic Scale Imaging of III-V Nanowire Surfaces”, *Nano Letters, vol.* 8 no. 11, pp. 3978–3982, 2008
[22] R. M. Feenstra, “Tunneling spectroscopy of the (110) surface of direct-gap III-V semiconductors”, *Phys. Rev. B*, vol. 50 no. 7, 4561-4570, 1994
[23] P. Caroff, K. A. Dick et al, “Controlled polytypic and twin-plane superlattices in III-V nanowires”, *Nature nanotechnology*, vol. 4, pp. 50-55, jan-2009.
[24] Ph. Ebert, “Nano-scale properties of defects in compound semiconductor surfaces”, *Surface Science Reports*, vol. 33, pp. 157-166, 1999
[25] E. Hilner, “Characterization of surfaces relevant to nanotechnology”, Lund University ISBN: 978-91-628-7965-5, pp. 1-9, Nov. 2009
[26] A. J Heinrich, M. Wenderoth, M. A Rosentreter, M. A Schneider and R. G Ulbrich, “Scanning tunneling microscopy of the atomic structure of the GaAs (110) surface at reduced tip sample separation”, *Appl. Phys. Lett*., vol. 70, pp. 449-451, 1997
[27] G. Binning and H. Roher, “Scanning Tunneling Microscopy”, *Helvetica Physica acta,* vol. 55, pp. 57-61, 1982
[28] J. Tersoff and D. R Hamann, “Theory of Application for the Scanning Tunneling Microscope”, *Physical Review letters*, vol. 50, pp. 1998-2001, 1983
[29] J. Tersoff and D. R Hamann, “Theory of Application for the Scanning Tunneling Microscope”, *Physical Review B*, vol. 31, pp. 805-813, 1985
[30] C. M. Lieber, “Semiconductor nanowires: A platform for nanoscience and nanotechnology”, *MRS Bulletin*, vol. 36, pp. 1052-1062, Dec 2011.
[31] Y. Li, F. Qian, J. Xiang and C. M. Lieber, “Nanowire electronic and optoelectronic devices”, Materialstoday, vol. 9, no. 10, pp. 18-27, Oct. 2006.

Acknowledgements

The possibility to write this thesis depends crucially on a number of people, to whom I would like to express my gratitude.

First of all I want to say thank you to my supervisor Anders Mikkelsen for making it possible to perform the experiments in the first place and for being available to answer questions and offer guidance.

I'm greatly indebted to Martin Hjort for teaching me the practical STM work and for all his patient explanations regarding the STM, nanowires and semiconductors. A special thanks to you for your support and for answering any questions. I would also like to thank Johan Knutsson who also gave me the opportunity to ask questions. Both of you made it a pleasant time in the lab.

I would like also like to acknowledge Sebastian Lehmann for providing the studied high quality nanowire samples. Not to be forgotten, everyone at the division for not only providing a friendly and inspiring atmosphere but also for bringing home-baked cake for the meetings.